ACS APPLIED MATERIALS & INTERFACES

Research Article

Cite This: ACS Appl. Mater. Interfaces 2017, 9, 41577-41585

www.acsami.org

Plasmonic Near-Field Localization of Silver Core–Shell Nanoparticle Assemblies via Wet Chemistry Nanogap Engineering

Ramesh Asapu,[†] Radu-George Ciocarlan,[‡] Nathalie Claes,[§] Natan Blommaerts,[†] Matthias Minjauw,[∥] Tareq Ahmad,[∥] Jolien Dendooven,[∥] Pegie Cool,[‡] Sara Bals,[§] Siegfried Denys,[†] Christophe Detavernier,[∥] Silvia Lenaerts,[†] and Sammy W. Verbruggen*[,†,⊥]

[†]Department of Bioscience Engineering, Campus Groenenborger, University of Antwerp, Groenenborgerlaan 171, Antwerp 2020, Belgium

[‡]Department of Chemistry, Campus Drie Eiken, University of Antwerp, Antwerp 2610, Belgium

[§]Department of Physics, Campus Groenenborger, University of Antwerp, Antwerp 2020, Belgium

[∥]Department of Solid State Sciences, Ghent University, Ghent 9000, Belgium

[⊥]Center for Surface Chemistry and Catalysis, KU Leuven, Leuven 3000, Belgium

Supporting Information

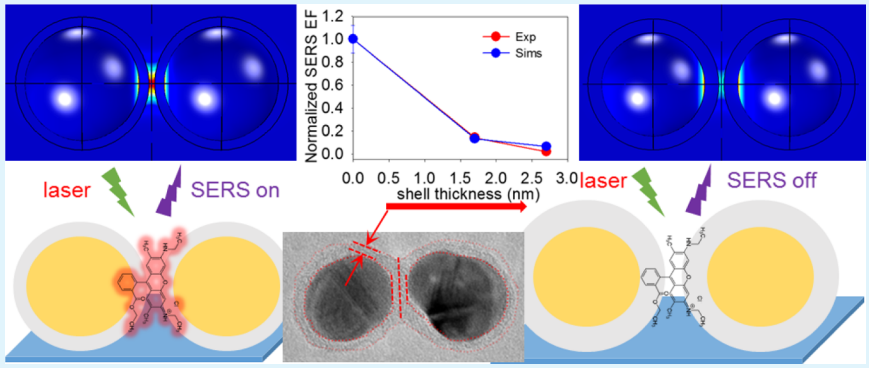

ABSTRACT: Silver nanoparticles are widely used in the field of plasmonics because of their unique optical properties. The wavelength-dependent surface plasmon resonance gives rise to a strongly enhanced electromagnetic field, especially at so-called hot spots located in the nanogap in-between metal nanoparticle assemblies. Therefore, the interparticle distance is a decisive factor in plasmonic applications, such as surface-enhanced Raman spectroscopy (SERS). In this study, the aim is to engineer this interparticle distance for silver nanospheres using a convenient wet-chemical approach and to predict and quantify the corresponding enhancement factor using both theoretical and experimental tools. This was done by building a tunable ultrathin polymer shell around the nanoparticles using the layer-by-layer method, in which the polymer shell acts as the separating interparticle spacer layer. Comparison of different theoretical approaches and corroborating the results with SERS analytical experiments using silver and silver–polymer core–shell nanoparticle clusters as SERS substrates was also done. Herewith, an approach is provided to estimate the extent of plasmonic near-field enhancement both theoretically as well as experimentally.

KEYWORDS: *surface plasmon resonance, silver, core–shell nanoparticles, SERS, layer-by-layer, nanogap, COMSOL Multiphysics*

1. INTRODUCTION

Noble metal nanoparticle synthesis has generated a significant amount of interest in the last few decades, especially in the plasmonics research domain. This is mainly because of the unique surface plasmon resonance (SPR) effect of noble metals resulting from their wavelength-dependent dielectric properties that give rise to a strongly enhanced near-electric field localized at the metal–dielectric interface.[1,2] The intense near-electric fields are the primary reason why plasmonic metal nanoparticles of Ag, Au, Pt, and so forth find wide application in multiple fields of research in diagnostic and optical applications such as biophotonics,[3−6] photocatalysis,[7−15] photovoltaics,[16−20] and surface-enhanced Raman spectroscopy (SERS).[21−26] Moreover, the scope of application with respect to SERS alone is so vast, of which some of the important domains range from imaging of numerous chemical and biological molecules to single-molecule detection.[27−30] The plasmonic design of hot spots is of major importance in SERS,[31−33] as controlling the shape, size, and spacing of these noble metal nanoparticles through colloidal self-assembly, sputtering, and nanolitho-

Received: September 14, 2017
Accepted: November 9, 2017
Published: November 9, 2017

ACS Publications © 2017 American Chemical Society

DOI: 10.1021/acsami.7b13965
ACS Appl. Mater. Interfaces 2017, 9, 41577−41585

graphic techniques has boosted the usage of the noble metal nanoparticles in such systems.[34−37] Among the noble metals, which possess these unique dielectric properties, silver nanoparticles are highly preferred in SERS applications, where electromagnetic (EM) enhancement plays a critical role and is a major contributing factor.[31,35,38,39] This is because silver has a higher near-field enhancement factor (EF) compared to other plasmonic metals, and silver is also economically more favorable. However, the main drawback associated with silver nanoparticles is the lack of long-term stability and formation of a diffuse silver-oxide layer, which reduces the EM enhancement and has a detrimental effect on SERS.[40,41]

As a solution to this problem, a protective layer consisting of metal oxides, carbon, and carbon-based ligand or capping agents can be built around the particle, creating a core−shell structure with a silver core and a protective shell layer.[35,42−44] Nevertheless, these methods come with a caveat of shielding the intense electric fields at the near vicinity of the nanoparticle because these shells commonly range from a couple of nanometers to almost the size of the core particle itself or even larger. For plasmonic applications, such as SERS, in which EM enhancement is crucial, this concentrated near-electric field must be available for the adsorbed probe molecules to achieve a strong enhancement in the spectroscopic signal. In our previous work,[12] a simple yet versatile method to synthesize Ag@polymer core@shell nanospheres using the layer-by-layer (LbL) technique for small-sized silver nanospheres (<25 nm diameter) was presented by building an ultrathin polymer shell. The degree of freedom to control the thickness of the protective polymer shell on the subnanometer level per layer allowed us to regulate the localized near-electric field available at the surface of the core−shell nanoparticle.

In this study, we carry out an analysis of the near-field and optical properties of silver−polymer core−shell nanospheres using the Mie theory[45] and finite element method (FEM) and corroborate the findings with the SERS experiments. The Mie analytical solution for core−shell nanospheres or coated spheres (called BHCOAT in FORTRAN code by Bohren and Huffman[46]) was implemented in a MATLAB code developed by Adleman.[47] In another method, Maxwell's EM differential wave equations were solved and discretized in space of the computational domain for 3D models, using the FEM, in COMSOL Multiphysics. The results were compared with the experimental spectra, and the trend in red shift of the SPR peak was followed. These results provide a good estimate of the effective distance from the nanoparticle surface and the vicinity in which the enhanced near-electric fields are active for silver nanospheres. This is validated by Raman experiments by preparing SERS substrates using silver nanospheres and silver−polymer core−shell nanospheres and rhodamine 6G as the Raman probe dye molecule. Also the ultrathin polymer shell is shown to be insulating, thus inhibiting the charge-transfer effect that sometimes comes into play depending on the selectivity of the probe molecule adsorption on the surface of the nanoparticles. Therefore, charge transfer as a contributing factor could be ruled out. Consequently, we demonstrate that the loss of signal enhancement in SERS with increasing interparticle distance is a direct result of decreasing EM enhancement. This is supported by the theoretical near-field simulations performed in COMSOL Multiphysics. Building on the interesting findings of various researchers who have applied the Mie theoretical analysis to study near-field enhancement in their research,[2,34,48−50] this work extends the analysis with metal@polymer core−shell nanoassemblies and not only relies on the analytical solution of the Mie theory but also includes comparison with the experimental synthesis results, SERS experiments, and FEM-based field simulations.

2. EXPERIMENTAL METHODS

2.1. Synthesis of Silver−Polymer Core−Shell Nanoparticles. The preparation of silver−polymer core−shell nanoparticles was performed as reported in our previous work.[12] In brief, colloidal silver nanoparticles were prepared according to an established procedure by Bastús et al.[51] The particles were subsequently coated with alternate layers of positive- and negative-charged polyelectrolytes, using polyelectrolyte solutions of 5 g/L PAH [polyallylamine hydrochloride, molecular weight (MW) 17.5 kDa, Sigma-Aldrich] and 10 g/L PAA (polyacrylic acid, MW 2 kDa, Sigma-Aldrich), respectively. The deposition of one alternate layer each of PAH and PAA is called a bilayer, and this cycle was continued until four bilayers were deposited, that is, $Ag/(PAH/PAA)_4$, resulting in an eight-layered polymer shell in total. The aliquots stored after each layer deposition were labelled as Ag_L*X*, where *X* represents the layer number; for example, aliquots after four- and eight-layer depositions were labelled as Ag_L4 and Ag_L8, respectively, whereas bare silver nanoparticles were labelled as Ag_L0.

2.2. SERS. Rhodamine 6G (Sigma-Aldrich, fluorescence bioreagent) dye was used as the Raman probe molecule for SERS measurements, and all measurements were done using glass substrates. The substrates were cleaned in acidic piranha solution (1:3 by volume of concentrated H_2O_2/H_2SO_4), followed by thoroughly rinsing in Milli-Q water. The cleaned glass substrates were dried in a nitrogen stream and immersed in 30% methanolic solution of (3-aminopropyl)-triethoxysilane for at least 12 h. The substrates were rinsed with methanol and dried in a nitrogen stream, followed by drying at 100 °C for 30 min. These substrates were prepared for SERS measurements by drop-casting a mixture of known concentration of R6G (10 μL of 10^{-4} M) and silver nanospheres or silver−polymer core−shell nanospheres. All samples were allowed to dry in a desiccator for 1 full day before the measurement. All samples with bare silver and silver−polymer core−shell nanospheres were adjusted to the same concentration by dilution, and 1 mL of all solutions were concentrated to within 40 μL by centrifugation before the addition of the dye solution. With a colloidal concentration of 4×10^{11} NPs/mL, a rough estimation could be made that around 1500 R6G molecules per nanosphere are present in the concentrated 50 μL sample drop. A reference neat R6G Raman substrate was prepared by drop-casting 50 μL of 10^{-2} M pure R6G dye solution. Raman spectra were recorded multiple times at different locations for each sample, and the calculation of EFs is shown in the Supporting Information section and corresponding Table S1.

2.3. Characterization. UV−visible (UV−vis) absorption spectra were recorded with a Shimadzu 2501 spectrophotometer. Multiple scans were taken in the wavelength range of 300−700 nm with a resolution of 0.2 nm. An average was taken for three consecutive spectral measurements to accurately locate the SPR peak position. Transmission electron microscopy (TEM) measurements were performed using a FEI Tecnai transmission electron microscope operated at 200 kV. A small drop of the colloidal sample was absorbed for 5 min onto a QUANTIFOIL copper grid that was coated with a carbon film (3.19 nm). All Raman measurements were done using a HORIBA XploRA PLUS Raman microscope under the same conditions. A 532 nm diode-pumped solid-state laser with a power of 25 mW was used for excitation, and all spectra were collected with an accumulation time of 20 s. For the nanoscopic measurements using conductive atomic force microscopy (C-AFM), a dilute colloidal solution of silver−polymer core−shell nanoparticles was drop-casted on a substrate precoated with gold to attain monolayer coverage. Substrates were attached to a stainless steel sample plate using a conductive carbon tape. The sample was loaded in an Omicron VT XA ultrahigh vacuum atomic force microscope, which operates at a base

DOI: 10.1021/acsami.7b13965
ACS Appl. Mater. Interfaces 2017, 9, 41577−41585

pressure of 10^{-10} mbar. Durable B-doped full diamond tips were used for optimum electrical contact, reproducibility, and suitable tip resistance.

3. THEORETICAL CALCULATIONS

3.1. Mie Theory Analytical Solution. In 1908, Gustav Mie developed a theory to understand the various optical phenomena of scattering, absorption, and extinction for small colloidal gold nanoparticles suspended in water.[45] The mathematics behind the theory consists of determination of a series of coefficients to solve for the vector wave equations derived from Maxwell's EM wave theory, and it provided the first framework to compute scattering of light by small spherical particles. After decades of research and innovation, Mie theory is now applied in a much broader field, ranging from atmospheric science and metamaterials to engineering of plasmonics and near-field optics. Albeit, there is always some amount of assumption involved, for example, with respect to the nanoparticle shape. With a plethora of such simplifications, mathematical conjectures, analysis of pitfalls, and potpourri of solutions to the Mie theory, Bohren and Huffman compiled a work[46] in 1983, which is still highly regarded. The crucial step forward was the development of an algorithm, which simplifies the calculations, and it was compiled in FORTRAN code. This code was later implemented in different programs by many researchers, to such an extent that as of today, there are hundreds of open source codes, which help the nascent physicist to solve Mie equations analytically. In this work, the Mie solution was chosen for a coated sphere or core−shell nanosphere, developed as BHCOAT FORTRAN code by Bohren,[46] which was implemented in MATLAB by Adleman[47] in his doctoral thesis. In brief, the code solves for numerous coefficients and calculates the extinction and absorption coefficients for a homogenous sphere after the derivation of expressions for scattering and extinction coefficients. For more details on the code and the underlying equations, the reader is referred to the Supporting Information section.

When performing the analytical calculations, the dielectric data for silver, taken from the literature,[52−54] were implemented through a wavelength-dependent data function. Also, the data for water were taken from Segelstein[55] with a wavelength dependency, instead of using a constant value of 1.33. In the case of air as the surrounding medium, a constant refractive index of 1 was used, whereas for the polymer shell material, a constant value of 1.48 was taken from the literature.[56] A cubic spline function was implemented to plot the resulting efficiencies against the wavelength, and the SPR peak position wavelength was identified.

3.2. FEM. Over the last decade, the evolution of faster computational machines has facilitated the FEM to be highly useful to solve for the differential equations of Maxwell's EM theory in three dimensions. FEM has the advantage of a highly useful application in the coupling of fields and physical quantities and has the capability to solve for periodic structures and arbitrary shapes. The models involve differential equations that are solved in a three-dimensional (3D) domain and discretized in space using large meshing and have a minor drawback with respect to the computation time and large memory space requirement for complex 3D structures. But with proper usage of resources and improvisation of solver algorithms with latest versions of computational programs such as COMSOL Multiphysics, the complexity of 3D models is no longer a concern. In this work, we make use of the COMSOL wave optics module, in which Maxwell's wave equations are solved with respect to the scattered electric field. More details can be found in the Supporting Information section.

3D models of bare silver nanospheres and silver−polymer core−shell nanospheres with varying polymer shell thicknesses were built in wave optics physics in COMSOL Multiphysics (ver. 5.3). A z-axis polarized monochromatic plane wave propagating in the x-axis direction was solved for the scattered field in a wavelength domain study. The above equations were implemented in COMSOL by assigning the formulae to the corresponding variables; please refer to the Supporting Information section for a detailed explanation on modeling. To calculate the extinction and absorption efficiencies, the incident excitation wavelength of the monochromatic plane wave was varied in the range of 300−700 nm. COMSOL has inbuilt wavelength-dependent refractive index data in its material database, adapted from Johnson and Christy,[52] and the refractive index data for water are imported as cubic interpolated data from Segelstein.[55] The incident light wavelength is the same as the as the excitation laser wavelength of the Raman microscope used in the experiments, that is, 532 nm.

4. RESULTS AND DISCUSSION

The as-synthesized core−shell nanoparticles with a silver core and a polymer shell were characterized by UV−vis spectroscopy after each layer deposition (Figure 1a). The decrease in the intensity corresponds to loss of nanoparticles during the multiple cycles of washing and centrifuging. A clear red shift in the plasmon peak position upon addition of successive polyelectrolyte layers can be derived from Figure 1b, which is an indication of the gradual increase in the particle size because

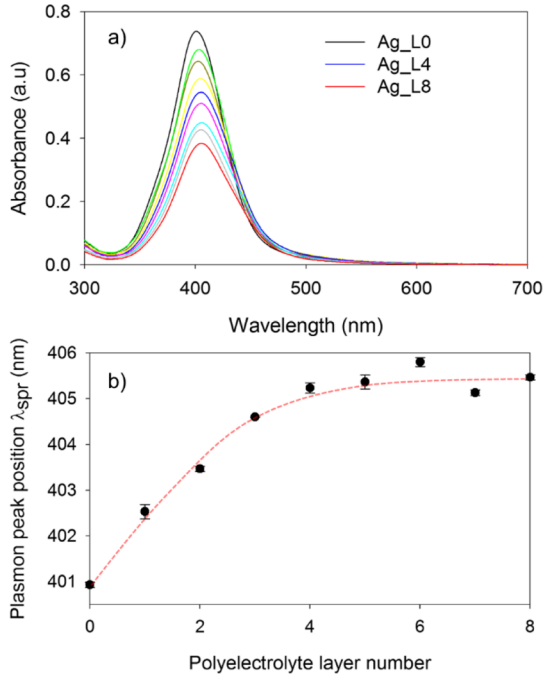

Figure 1. (a) UV−vis absorption spectra and (b) SPR peak position of silver core−polymer shell nanoparticles as a function of the number of encapsulating layers. The dotted red curve is a trend line of the shift in the plasmon peak position.

DOI: 10.1021/acsami.7b13965
ACS Appl. Mater. Interfaces 2017, 9, 41577−41585

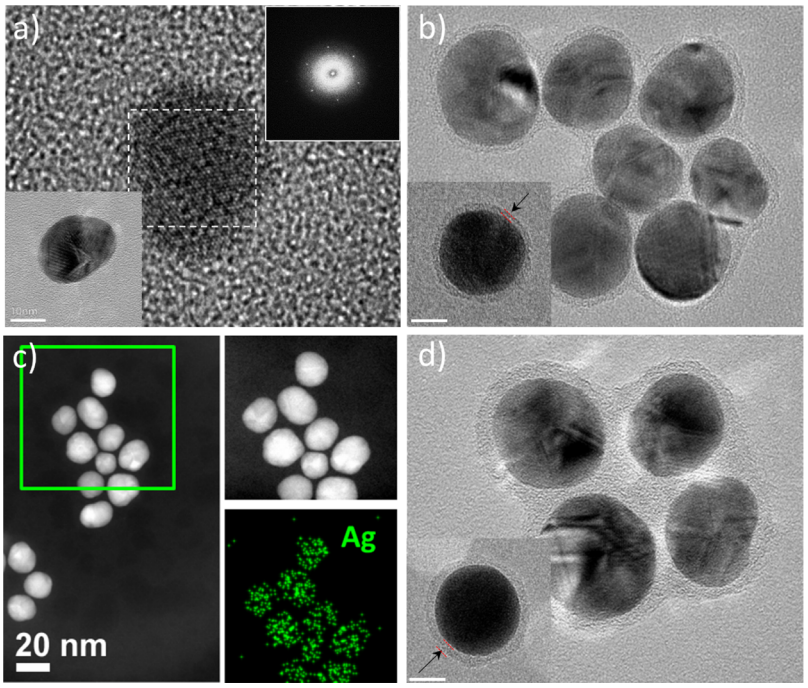

Figure 2. (a) High-resolution TEM image of a silver nanoparticle with the SAED pattern of silver in the top right corner; (b) BF-TEM images of Ag_L4: four-layered core−shell nanosphere with a shell thickness of 1.7 ± 0.4 nm; (c) high-angle annular dark field scanning transmission electron microscopy image of Ag_L4 core−shell nanosphere clusters with energy-dispersive X-ray map; (d) Ag_L8: eight-layered core−shell nanosphere with a shell thickness of 2.7 ± 0.6 nm. High-resolution BF-TEM images in the insets are isolated single core−shell nanoparticles with a scale bar corresponding to 10 nm in (a,b,d).

of an increase in the encapsulating polymer shell thickness as more polyelectrolyte layers are deposited.

Also, from bright-field TEM (BF-TEM) images in Figure 2, a gradual increase in the shell thickness could be observed, with no shell for the bare silver nanoparticles (Figure 2a) and formation of core−shell nanospheres Ag_L4 (Figure 2b,c) and Ag_L8 (Figure 2d) encapsulated by a thin shell of thickness 1.7 and 2.7 nm, respectively. The TEM images in Figure 2b,d represent the pattern in which the core−shell nanoparticles dry on a substrate. Even though the core−shell nanoparticles seem to be aggregated when dried, the spacing between the adjacent particles is controlled by the polymer layer shell thickness; whereas for bare silver nanoparticles, this kind of spacing is not present, and the nanoparticles aggregate immediately after the addition into the Raman probe molecule solution.

The difference in color as seen from Figure S4 for bare and encapsulated silver nanoparticles before and after drying in a desiccator is a clear evidence. The absorbance calculated from the Mie analytical MATLAB code and COMSOL was plotted with the experimental absorption spectrum, as shown in Figure 3. The optical constant data used for these calculations were taken from the literature, and because there are numerous well-known datasets, we have primarily used silver permittivity data from Johnson & Christy,[52] Palik,[53] and Ripken[54] represented as Mie_J&C, Mie_Palik, and Mie_Ripken, respectively, in the plots for convenience. For any of these datasets, a clear red shift of the SPR peak position is observed after encapsulation of the silver nanoparticles with a 2.7 nm thick polymer shell (Figure 3b versus Figure 3a).

There seems to be a striking difference in the absolute value of the peak position as well as the shape of the spectrum when using multiple datasets as compared to experimental spectra for both bare Ag nanoparticle and core−shell nanoparticles. This

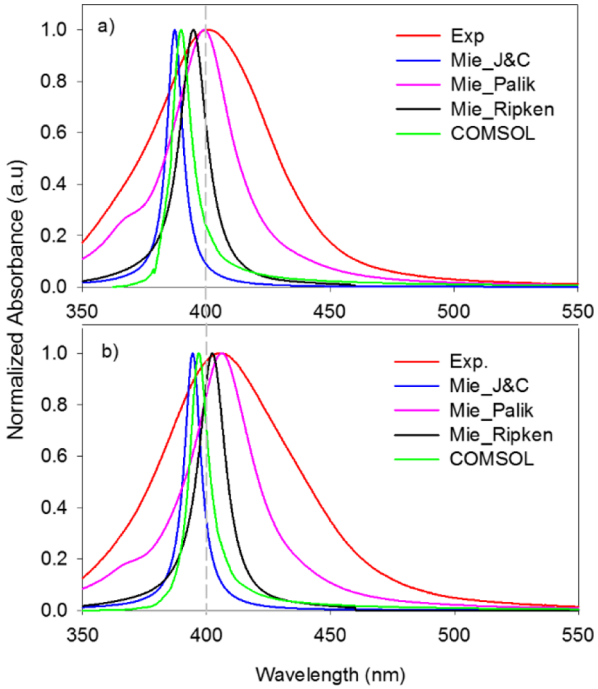

Figure 3. Comparison of normalized UV−vis experimental spectra with the calculated theoretical absorption efficiencies for (a) bare silver nanospheres and (b) silver−polymer core−shell nanospheres with 2.7 nm shell thickness (Ag_L8).

can be attributed to the fact that in the Mie analytical calculations and COMSOL model, the nanoparticles are assumed perfectly spherical, of a single size, and highly monodisperse, which is rarely the case in a true experimental

DOI: 10.1021/acsami.7b13965
ACS Appl. Mater. Interfaces 2017, 9, 41577−41585

scenario. The polydispersity of synthesized colloidal nanoparticles is related to the full peak width at half-maximum of the spectra, which is not taken into account in either the Mie calculations or the COMSOL model. These assumptions will always lead to plasmon band narrowing and a minor shift in the band position for analytical calculations, which is well in line with the literature.[34,48,57] It is also important to note that the datasets used from different researchers vary because the experimental methods used to generate the optical constants are quite different. In addition, each method uses independent corrections in the mean free path of electrons for the calculations of the dielectric parameters, in cases where the particle sizes get too small. However, the trend in the red shift of the plasmon peak position with increased shell thickness is mostly in agreement with the experiments (Figure 4). Still, for a

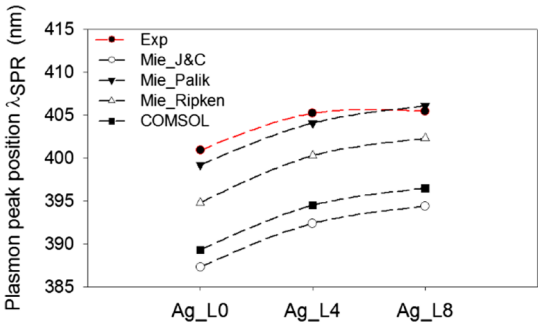

Figure 4. Comparison of experimental spectra with the theoretical calculations in water, showing the plasmon peak position of bare (Ag_L0) and core–shell nanospheres (Ag_L4 and Ag_L8).

shell thickness of 2.7 nm (Ag_L8), the red shift becomes less substantial than for thinner shells (also clear from the plateau that is reached in Figure 1b). The theoretical calculations on the other hand still show a significant red shift with an increase in the polymer shell thickness. Such an experimental leveling off of the red shift is expected for core–shell nanoparticles with thick optically transparent shells, as the shift in the plasmon peak becomes insignificant.[57] It also depends on the refractive index of the surrounding medium, as obviously noticeable from the theoretical equations (Supporting Information). Figure 5 depicts the trend in red shift of the plasmon peak with increasing shell thickness, calculated for air and water as surrounding media. This implies that, as the ratio of the

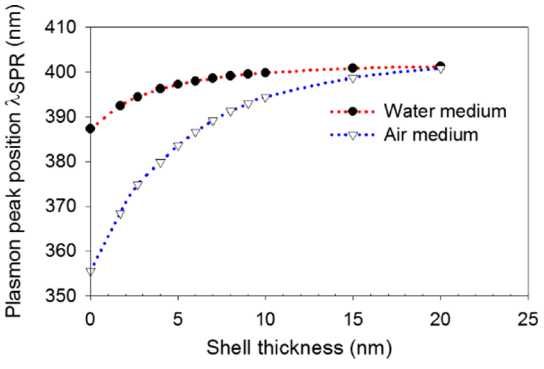

Figure 5. Mie analytical calculations showing the red shift in the plasmon peak position as a function of increasing polymer shell thickness for core–shell nanospheres in air and water as the surrounding media.

refractive indices of the shell versus the surrounding medium becomes closer to unity, the red shift in the plasmon peak as a result of increasing shell thickness will slowly disappear. In other words, there would be a blue shift in the plasmon peak position if the core–shell nanoparticles were suspended in a medium with a refractive index that is higher than that of the shell. Among all datasets, the Mie_Palik dataset seems to match best with the experimental red shift (Figure 4). For the experimental dataset, a plateau value is reached, which is not yet the case for the theoretical calculations in this range of shell thickness. This deviation can potentially be attributed to the use of a constant refractive index for a composite of polyelectrolyte layers in the calculations. From a practical point of view, small deviations in the shell thickness or imperfections within the polymer composite are also possible. Overall, it should be clear that the shell thickness is a crucial factor for plasmonic core–shell nanoparticles as it has a significant effect on both optical as well as near-field properties.

As discussed earlier, for plasmonic nanomaterials such as silver nanospheres, enhanced near-fields are the main asset for plasmonic applications, such as SERS. Therefore, it is important to study how the shell affects these near-field properties. In addition, another main scope of this work is to find out the distance or vicinity from the surface of the nanosphere to which the enhanced near-field is confined. For this specific purpose, SERS is used as an experimental tool to verify the resulting plasmonic enhancement when applying polymer shells of varying thicknesses as an interface building material to adjust the near-field localization of silver nanospheres. In other words, by building polymer shells with high control over the resulting thickness, the nanogap between two adjacent silver cores can be tuned, and the resulting hot spot effect can be regulated. As explained in the experimental section, SERS substrates are prepared using bare silver nanospheres (Ag_L0) and silver–polymer core–shell nanospheres with two different shell thicknesses (Ag_L4 and Ag_L8).

Figure 6a shows the SERS measurements of different substrates, and significant enhancements are found for 10^{-4} M R6G in the presence of both bare silver nanospheres (Ag_L0) and silver–polymer core–shell nanospheres with a shell thickness of 1.7 nm (Ag_L4). The Raman intensity for the neat R6G substrate of 0.01 M R6G is amplified 5 times for better visualization in the common intensity scale. However, little-to-no enhancement/signal could be detected for R6G in the presence of a core–shell nanoparticle with a shell thickness of 2.7 nm (Ag_L8). The decrease in the experimental SERS EFs calculated from the Raman measurements are shown in Figure 6b. The EFs are calculated by using the integrated intensity of the 1365 cm^{-1} band of the C–C/C–N stretch of the R6G molecule at which major enhancement in signal is recorded. From the measurements, it can be inferred that a significantly high enhancement (EF $\approx 1.2 \times 10^4$) is shown by bare silver nanospheres, and a considerable decline in the EF ($\sim 1.8 \times 10^3$) is observed when Ag nanospheres coated with a shell thickness of 1.7 nm are used. Also, when the silver nanoparticles are coated with a shell of thickness 2.7 nm or more, insignificant experimental enhancement of the Raman signal could be achieved.

This indicates that the shell thickness, that is, the distance from the surface of the Ag nanoparticles, plays a major role in regulating the enhanced near-electric fields available at the surface of the nanoparticle. In other words, tuning the distance between the Raman probe molecules and the surface of the Ag

DOI: 10.1021/acsami.7b13965
ACS Appl. Mater. Interfaces 2017, 9, 41577–41585

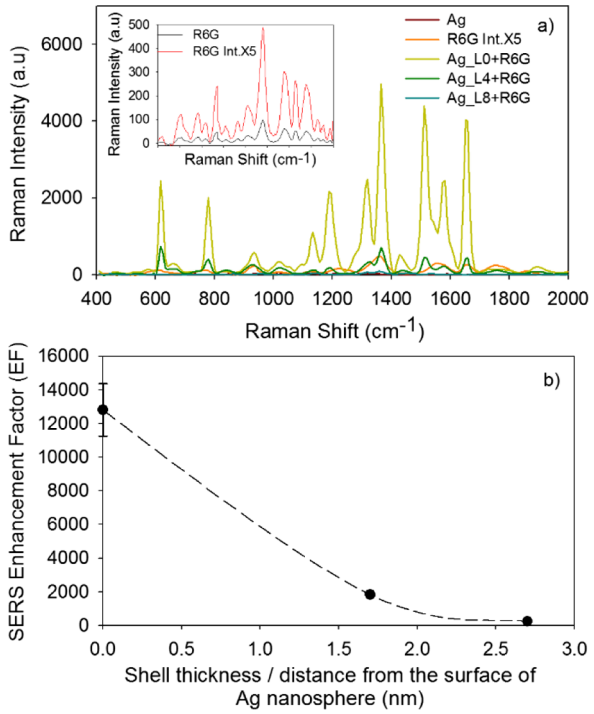

Figure 6. (a) SERS measurements of pure Ag nanospheres, 10 mM R6G (intensity amplified 5 times, original and amplified spectra shown in the inset) and 0.1 mM R6G with substrates of Ag nanospheres, Ag_L4, and Ag_L8 core−shell nanospheres; (b) SERS EF as a function of the distance from the silver nanosphere surface.

nanospheres is achieved by controlling the thickness of the polyelectrolyte layers. Therefore, investigating the effect of shell thickness on the near-field enhancement through field simulations using FEM will be very helpful. In this work, COMSOL Multiphysics was used to perform the near-field simulations using FEM, and the results are shown in Figure 7. The experimental SERS EM enhancement can be a result of near-field generated by either a single nanosphere or the hot spots created in-between the nanogap of nanoparticle assemblies. Analyzing the field simulation maps in Figure 7a and the quantified theoretical EFs (using the $|E/E_0|^4$ estimation,[25] see the Supporting Information Figure S3), the maximum EF is found to be only on the order of 10^2 for a single Ag nanosphere and drops significantly with increase of the shell thickness. Such low theoretical EFs do not match the high experimentally observed EF. So, the high EFs achieved from SERS experiments can only be explained by a major contribution from the intense near-fields produced in the hot spots,[30,31,58] that is, the nanogaps between the nanoparticles. It can be assumed that the hot spot in the nanosphere dimer is of the same order of magnitude as in nanoparticle clusters, with the exception of the formation of high spatial localization in 3D structures. This assumption is mainly for ease of visualization and analysis of hot spots in field simulation maps. In addition, the magnitude of the near-field in the nanogaps of dimers, trimers, or tetramers is not significantly different, as evidenced by theoretical simulations (Figure 8). The field enhancement maps for the dimer systems, with a nanogap of 1 nm, are shown in Figure 7b, and one can observe that the hot spot intensity decreases for a shell thickness of 1.7 nm and becomes almost nonexistent for a shell thickness of 2.7 nm. This is in good agreement with the experimental observation of the SERS EFs, which is also observed from Figure 9 that shows a comparison between the theoretical and experimental SERS EFs. Moreover, there is a very good match for the decay ratio of SERS EF with increasing shell thickness. To estimate the theoretical EF from simulations, a nanogap of 2 nm between two nanoparticles is considered to match the condition when one R6G dye molecule is adsorbed on the adjacent particles, providing a spacing layer.

Eventually these analyses provide a more realistic picture that, beyond a distance/vicinity of 1.7 nm from the surface of nanoparticle, the EM enhancement becomes negligible. These results are in line with the literature,[26,40,59] where it has been reported that within 1−2 nm from the surface of the plasmonic nanoparticle, the enhancement is radically reduced. There is a possibility that an ultrathin polymer layer of 1.7 nm may be inherently enhancing the Raman signal through chemical enhancement when the adsorbed R6G molecule interacting with the polymer chain allows for a quick charge transfer. To investigate this potential contribution, C-AFM measurements were performed to find the charge-transfer properties of silver−polymer core−shell nanoparticles. The reason for using C-AFM to determine the electrical properties of the core−shell

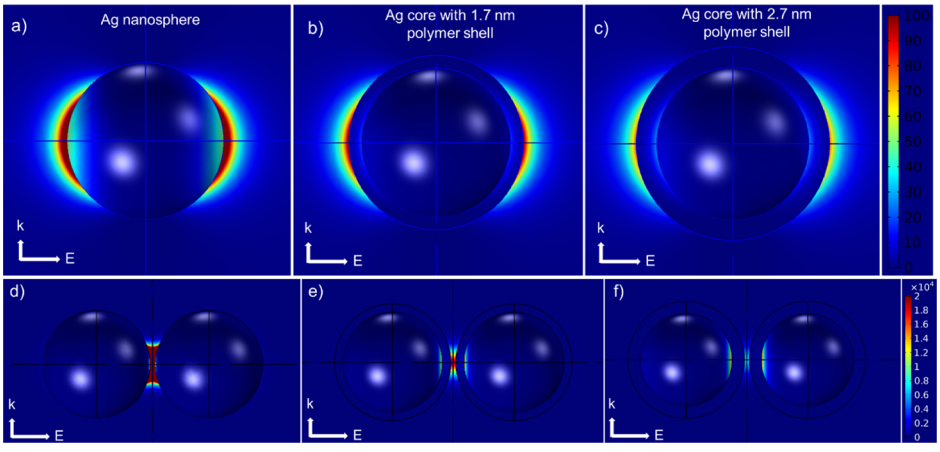

Figure 7. (a) Near-field simulation maps at the Raman excitation wavelength of 532 nm in air for (a) Ag nanospheres, for silver−polymer core−shell nanospheres with a shell thickness of (b) 1.7 nm (Ag_L4) and (c) 2.7 nm (Ag_L8), and (d−f) the corresponding dimers of the nanospheres. The scale ($|E/E_0|^4$) is normalized at 100 for single nanospheres and 2×10^4 for dimers for better visualization of the enhanced fields.

DOI: 10.1021/acsami.7b13965
ACS Appl. Mater. Interfaces 2017, 9, 41577−41585

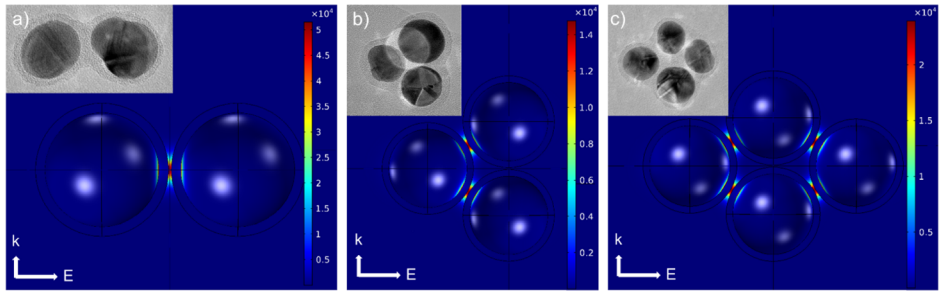

Figure 8. Field enhancement maps for (a) dimer, (b) trimer, and (c) tetramer silver−polymer core−shell nanoparticle clusters with TEM inset images for representation. The color legends are in the scale of $|E/E_0|^4$, representing the magnitude of maximum theoretical SERS EF.

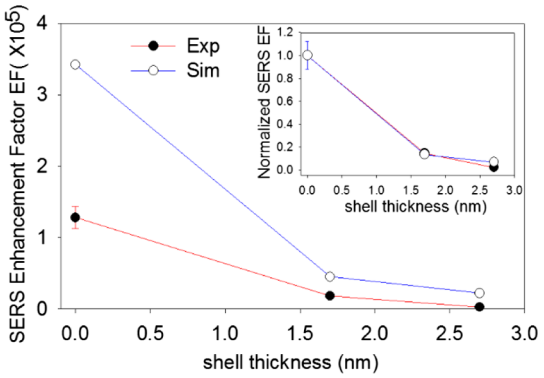

Figure 9. Comparison of theoretical and experimental SERS EFs. The inset shows the comparison with a normalized EF.

nanoparticles is that the polymer blends have unique electrical properties depending on the type of polymers used. Merely measuring the current−voltage (I−V) properties of the as-prepared silver−polymer core−shell nanocluster film can lead to false interpretations, when using a typical four-point probe method to determine the resistivity. This is because in a dried nanocluster film, the polymer shells of adjacent nanoparticles are in contact, and the resulting resistance is in fact that of a long nanoparticle chain. So, a more robust methodology is adapted by immersing a gold-coated Si wafer in a dilute colloidal solution of silver−polymer core−shell nanoparticles to make sure single isolated core−shell nanoparticles could be imaged by AFM. This is followed by applying a voltage through the conductive cantilever tip of the AFM, and the detected current levels indicate the resistance of the core−shell nanoparticle on the gold substrate. From Figure 10, it can be observed that a core−shell nanoparticle with a shell thickness of 1.7 nm is highly insulating and resists charge transfer. Both particles in the AFM surface image showed no passage of current with increase in voltage until the AFM cantilever tip tunneled through the particle and made contact with the gold substrate underneath. This is a classic tunneling I−V profile for high resistance or insulating materials. This measurement rules out chemical enhancement due to charge transfer through the ultrathin polymer shell. This also supports the fundamental theory that near-field or EM enhancement is the major mechanism responsible for SERS as established in the literature.[21−23,60]

As a final remark, it should be noted that because of the size and shape dependence of SPR on metal nanoparticles such as silver, this can and will affect the hot spots and correlated intensity enhancement that can be achieved in SERS. Additionally, using different polymer materials for the shell (either insulating or conductive) will also have an impact as long as there is a significant change in the refractive index of the polymer materials used. Nonetheless, the replication of the LbL procedure and resulting parameters of the shell thickness and the corresponding red shifts confirm excellent repeatability (Supporting Information Figure S5). The findings presented in this study, based on an average silver nanoparticle size of 20 nm and its corresponding polymer combinations to tune the nanogap in-between should therefore be regarded as a more generic approach to fine-tune the near-field localization of plasmonic nanoparticles for various other core−shell composite nanostructures.

5. CONCLUSIONS

This study demonstrates how experimental methods in conjunction with theoretical simulations can act as a vital mechanistic tool to understand the plasmonic properties of silver nanoparticles. In this way, the effect of shell thickness on the optical properties of core−shell nanoparticles and nano-

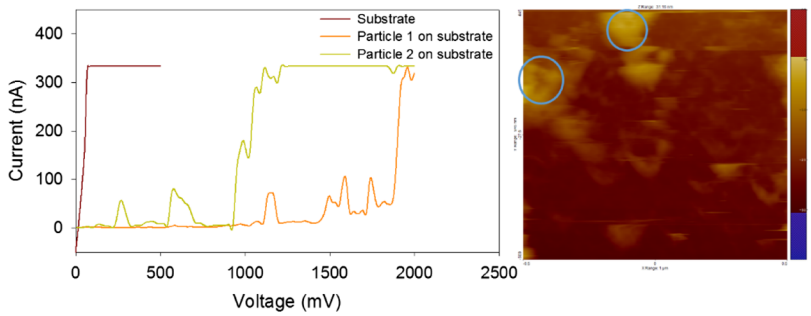

Figure 10. C-AFM measurements performed on the gold substrate and on two core−shell nanospheres deposited on the substrate; the surface image shows the location of two particles.

DOI: 10.1021/acsami.7b13965
ACS Appl. Mater. Interfaces 2017, 9, 41577−41585

particle assemblies is thoroughly examined. The application of a spacer layer through wet chemical methods such as LbL can be used to effectively engineer the size of the nanogap in-between adjacent particles. This is important as it is shown that the distance from the particle core greatly affects the near-field and the resulting SERS enhancement. Comparison with theoretical FEM field simulations indicates that experimentally obtained EFs in SERS are mainly determined by the enhanced near-electric field generated at the hot spot zones in-between particles, of which the nanogap can be regulated through the thickness of the spacer shell layer. These tools and insights will aid in more straightforward nanoengineering of substrates for plasmonic applications to target the localized vicinity of field enhancement and make use of hot spot effects of such plasmonic nanoparticles. Moreover, it will help identify and engineer the optimal interparticle distance, customized to a particular plasmonic application.

■ ASSOCIATED CONTENT

Supporting Information

The Supporting Information is available free of charge on the ACS Publications website at DOI: 10.1021/acsami.7b13965.

Mie theory analytical calculations, FEM modeling in COMSOL Multiphysics, and SERS calculations (PDF)

■ AUTHOR INFORMATION

Corresponding Author

*E-mail: sammy.verbruggen@uantwerp.be.

ORCID

Matthias Minjauw: 0000-0003-3620-8949
Pegie Cool: 0000-0002-6632-2243
Sara Bals: 0000-0002-4249-8017
Sammy W. Verbruggen: 0000-0003-2372-9630

Author Contributions

The manuscript was written through contributions of all authors. All authors have given approval to the final version of the manuscript.

Notes

The authors declare no competing financial interest.

■ ACKNOWLEDGMENTS

M.M., J.D., and S.W.V. acknowledge FWO Vlaanderen for the financial support through a research fellowship. C.D. wishes to thank the Hercules foundation for the financial support (SPINAL). P.C. and R.-G.C. acknowledge financial support by FWO Vlaanderen (project no. G038215N). N.C. and S.B. acknowledge the financial support from the European Research Council (ERC starting grant #335078-COLOURATOM).

■ REFERENCES

(1) Murray, W. A.; Barnes, W. L. Plasmonic Materials. *Adv. Mater.* **2007**, *19*, 3771−3782.

(2) Hutter, T.; Huang, F. M.; Elliott, S. R.; Mahajan, S. Near-Field Plasmonics of an Individual Dielectric Nanoparticle above a Metallic Substrate. *J. Phys. Chem. C* **2013**, *117*, 7784−7790.

(3) West, J. L.; Halas, N. J. Engineered Nanomaterials for Biophotonics Applications: Improving Sensing, Imaging, and Therapeutics. *Annu. Rev. Biomed. Eng.* **2003**, *5*, 285−292.

(4) Haes, A. J.; Haynes, C. L.; McFarland, A. D.; Schatz, G. C.; Van Duyne, R. P.; Zou, S. Plasmonic Materials for Surface-Enhanced Sensing and Spectroscopy. *MRS Bull.* **2005**, *30*, 368−375.

(5) Khlebtsov, N. G. Optics and Biophotonics of Nanoparticles with a Plasmon Resonance. *Quantum Electron.* **2008**, *38*, 504−529.

(6) Willets, K. A.; Van Duyne, R. P. Localized Surface Plasmon Resonance Spectroscopy and Sensing. *Annu. Rev. Phys. Chem.* **2007**, *58*, 267−297.

(7) Verbruggen, S. W. TiO2 Photocatalysis for the Degradation of Pollutants in Gas Phase: From Morphological Design to Plasmonic Enhancement. *J. Photochem. Photobiol., C* **2015**, *24*, 64−82.

(8) Boerigter, C.; Campana, R.; Morabito, M.; Linic, S. Evidence and Implications of Direct Charge Excitation as the Dominant Mechanism in Plasmon-Mediated Photocatalysis. *Nat. Commun.* **2016**, *7*, 10545.

(9) Linic, S.; Christopher, P.; Ingram, D. B. Plasmonic-Metal Nanostructures for Efficient Conversion of Solar to Chemical Energy. *Nat. Mater.* **2011**, *10*, 911−921.

(10) Ingram, D. B.; Christopher, P.; Bauer, J. L.; Linic, S. Predictive Model for the Design of Plasmonic Metal/Semiconductor Composite Photocatalysts. *ACS Catal.* **2011**, *1*, 1441−1447.

(11) Verbruggen, S. W.; Keulemans, M.; Goris, B.; Blommaerts, N.; Bals, S.; Martens, J. A.; Lenaerts, S. Plasmonic "rainbow" Photocatalyst with Broadband Solar Light Response for Environmental Applications. *Appl. Catal., B* **2016**, *188*, 147−153.

(12) Asapu, R.; Claes, N.; Bals, S.; Denys, S.; Detavernier, C.; Lenaerts, S.; Verbruggen, S. W. Silver-Polymer Core-Shell Nanoparticles for Ultrastable Plasmon-Enhanced Photocatalysis. *Appl. Catal., B* **2017**, *200*, 31−38.

(13) Verbruggen, S. W.; Keulemans, M.; Filippousi, M.; Flahaut, D.; Van Tendeloo, G.; Lacombe, S.; Martens, J. A.; Lenaerts, S. Plasmonic Gold−Silver Alloy on TiO2 Photocatalysts with Tunable Visible Light Activity. *Appl. Catal., B* **2014**, *156−157*, 116−121.

(14) Blommaerts, N.; Asapu, R.; Claes, N.; Bals, S.; Lenaerts, S.; Verbruggen, S. W. Gas Phase Photocatalytic Spiral Reactor for Fast and Efficient Pollutant Degradation. *Chem. Eng. J.* **2017**, *316*, 850−856.

(15) Awazu, K.; Fujimaki, M.; Rockstuhl, C.; Tominaga, J.; Murakami, H.; Ohki, Y.; Yoshida, N.; Watanabe, T. A Plasmonic Photocatalyst Consisting of Silver Nanoparticles Embedded in Titanium Dioxide. *J. Am. Chem. Soc.* **2008**, *130*, 1676−1680.

(16) Atwater, H. A.; Polman, A. Plasmonics for Improved Photovoltaic Devices. *Nat. Mater.* **2010**, *9*, 205−213.

(17) Brown, M. D.; Suteewong, T.; Kumar, R. S. S.; D'Innocenzo, V.; Petrozza, A.; Lee, M. M.; Wiesner, U.; Snaith, H. J. Plasmonic Dye-Sensitized Solar Cells Using Core−Shell Metal−Insulator Nanoparticles. *Nano Lett.* **2011**, *11*, 438−445.

(18) Sharma, M.; Pudasaini, P. R.; Ruiz-Zepeda, F.; Vinogradova, E.; Ayon, A. A. Plasmonic Effects of Au/Ag Bimetallic Multispiked Nanoparticles for Photovoltaic Applications. *ACS Appl. Mater. Interfaces* **2014**, *6*, 15472−15479.

(19) Clavero, C. Plasmon-Induced Hot-Electron Generation at Nanoparticle/metal-Oxide Interfaces for Photovoltaic and Photocatalytic Devices. *Nat. Photonics* **2014**, *8*, 95−103.

(20) Sandén, S.; Akitsu, K.; Törngren, B.; Ylinen, A.; Smått, J.-H.; Kubo, T.; Matsumura, M.; Otani, N.; Segawa, H.; Österbacka, R. Plasmon-Enhanced Polymer-Sensitized Solar Cells. *J. Phys. Chem. C* **2015**, *119*, 5570−5576.

(21) Sharma, B.; Frontiera, R. R.; Henry, A.-I.; Ringe, E.; Van Duyne, R. P. SERS: Materials, Applications, and the Future. *Mater. Today* **2012**, *15*, 16−25.

(22) Schlücker, S. Surface-Enhanced Raman Spectroscopy: Concepts and Chemical Applications. *Angew. Chem., Int. Ed.* **2014**, *53*, 4756−4795.

(23) McFarland, A. D.; Young, M. A.; Dieringer, J. A.; Van Duyne, R. P. Wavelength-Scanned Surface-Enhanced Raman Excitation Spectroscopy. *J. Phys. Chem. B* **2005**, *109*, 11279−11285.

(24) Leopold, N.; Lendl, B. A New Method for Fast Preparation of Highly Surface-Enhanced Raman Scattering (SERS) Active Silver Colloids at Room Temperature by Reduction of Silver Nitrate with Hydroxylamine Hydrochloride. *J. Phys. Chem. B* **2003**, *107*, 5723−5727.

DOI: 10.1021/acsami.7b13965
ACS Appl. Mater. Interfaces 2017, 9, 41577−41585

(25) Stiles, P. L.; Dieringer, J. A.; Shah, N. C.; Van Duyne, R. P. Surface-Enhanced Raman Spectroscopy. *Annu. Rev. Anal. Chem.* **2008**, *1*, 601−626.
(26) Dieringer, J. A.; McFarland, A. D.; Shah, N. C.; Stuart, D. A.; Whitney, A. V.; Yonzon, C. R.; Young, M. A.; Zhang, X.; Van Duyne, R. P. Introductory Lecture: Surface Enhanced Raman Spectroscopy: New Materials, Concepts, Characterization Tools, and Applications. *Faraday Discuss.* **2006**, *132*, 9−26.
(27) Lim, D.-K.; Jeon, K.-S.; Kim, H. M.; Nam, J.-M.; Suh, Y. D. Nanogap-Engineerable Raman-Active Nanodumbbells for Single-Molecule Detection. *Nat. Mater.* **2010**, *9*, 60−67.
(28) Radziuk, D.; Moehwald, H. Prospects for Plasmonic Hot Spots in Single Molecule SERS towards the Chemical Imaging of Live Cells. *Phys. Chem. Chem. Phys.* **2015**, *17*, 21072−21093.
(29) Liu, R.; Liu, B.; Guan, G.; Jiang, C.; Zhang, Z. Multilayered Shell SERS Nanotags with a Highly Uniform Single-Particle Raman Readout for Ultrasensitive Immunoassays. *Chem. Commun.* **2012**, *48*, 9421−9423.
(30) Blackie, E. J.; Ru, E. C. L.; Etchegoin, P. G. Single-Molecule Surface-Enhanced Raman Spectroscopy of Nonresonant Molecules. *J. Am. Chem. Soc.* **2009**, *131*, 14466−14472.
(31) Xu, H.; Aizpurua, J.; Käll, M.; Apell, P. Electromagnetic Contributions to Single-Molecule Sensitivity in Surface-Enhanced Raman Scattering. *Phys. Rev. E: Stat. Phys., Plasmas, Fluids, Relat. Interdiscip. Top.* **2000**, *62*, 4318−4324.
(32) Kleinman, S. L.; Frontiera, R. R.; Henry, A.-I.; Dieringer, J. A.; Van Duyne, R. P. Creating, Characterizing, and Controlling Chemistry with SERS Hot Spots. *Phys. Chem. Chem. Phys.* **2013**, *15*, 21−36.
(33) Li, W.; Camargo, P. H. C.; Lu, X.; Xia, Y. Dimers of Silver Nanospheres: Facile Synthesis and Their Use as Hot Spots for Surface-Enhanced Raman Scattering. *Nano Lett.* **2009**, *9*, 485−490.
(34) Kelly, K. L.; Coronado, E.; Zhao, L. L.; Schatz, G. C. The Optical Properties of Metal Nanoparticles: The Influence of Size, Shape, and Dielectric Environment. *J. Phys. Chem. B* **2003**, *107*, 668−677.
(35) Radziuk, D.; Möhwald, H. Surpassingly Competitive Electromagnetic Field Enhancement at the Silica/silver Interface for Selective Intracellular Surface Enhanced Raman Scattering Detection. *ACS Nano* **2015**, *9*, 2820−2835.
(36) Chan, G. H.; Zhao, J.; Hicks, E. M.; Schatz, G. C.; Van Duyne, R. P. Plasmonic Properties of Copper Nanoparticles Fabricated by Nanosphere Lithography. *Nano Lett.* **2007**, *7*, 1947−1952.
(37) Stamplecoskie, K. G.; Scaiano, J. C.; Tiwari, V. S.; Anis, H. Optimal Size of Silver Nanoparticles for Surface-Enhanced Raman Spectroscopy. *J. Phys. Chem. C* **2011**, *115*, 1403−1409.
(38) Gill, R.; Tian, L. J.; Somerville, W. R. C.; Ru, E. C. L.; van Amerongen, H.; Subramaniam, V. Silver Nanoparticle Aggregates as Highly Efficient Plasmonic Antennas for Fluorescence Enhancement. *J. Phys. Chem. C* **2012**, *116*, 16687−16693.
(39) White, P.; Hjortkjaer, J. Preparation and Characterisation of a Stable Silver Colloid for SER(R)S Spectroscopy. *J. Raman Spectrosc.* **2014**, *45*, 32−40.
(40) Han, Y.; Lupitskyy, R.; Chou, T.-M.; Stafford, C. M.; Du, H.; Sukhishvili, S. Effect of Oxidation on Surface-Enhanced Raman Scattering Activity of Silver Nanoparticles: A Quantitative Correlation. *Anal. Chem.* **2011**, *83*, 5873−5880.
(41) Erol, M.; Han, Y.; Stanley, S. K.; Stafford, C. M.; Du, H.; Sukhishvili, S. SERS Not To Be Taken for Granted in the Presence of Oxygen. *J. Am. Chem. Soc.* **2009**, *131*, 7480−7481.
(42) Yang, D.; Xia, L.; Zhao, H.; Hu, X.; Liu, Y.; Li, J.; Wan, X. Preparation and Characterization of an Ultrathin Carbon Shell Coating a Silver Core for Shell-Isolated Nanoparticle-Enhanced Raman Spectroscopy. *Chem. Commun.* **2011**, *47*, 5873−5875.
(43) Li, D.; Wu, S.; Wang, Q.; Wu, Y.; Peng, W.; Pan, L. Ag@C Core−Shell Colloidal Nanoparticles Prepared by the Hydrothermal Route and the Low Temperature Heating−Stirring Method and Their Application in Surface Enhanced Raman Scattering. *J. Phys. Chem. C* **2012**, *116*, 12283−12294.
(44) Liu, T.-M.; Yu, J.; Chang, C. A.; Chiou, A.; Chiang, H. K.; Chuang, Y.-C.; Wu, C.-H.; Hsu, C.-H.; Chen, P.-A.; Huang, C.-C. One-Step Shell Polymerization of Inorganic Nanoparticles and Their Applications in SERS/nonlinear Optical Imaging, Drug Delivery and Catalysis. *Sci. Rep.* **2015**, *4*, 05593.
(45) Mie, G. Beitrage Zur Optik Truber Medien, Speziell Kolloidaler Metallosungen. *Ann. Phys.* **1908**, *330*, 377−445.
(46) Bohren, C. F.; Huffman, D. R. *Absorption and Scattering of Light by Small Particles*; Bohren, C. F., Huffman, D. R., Eds.; Wiley-VCH Verlag GmbH: Weinheim, Germany, 1998.
(47) Adleman, J. R. Plasmonic Nanoparticles for Optofluidic Applications. Ph.D. Thesis, California Institute for Technology, California, USA, 2009.
(48) Kim, Y.; Johnson, R. C.; Li, J.; Hupp, J. T.; Schatz, G. C. Synthesis, Linear Extinction, and Preliminary Resonant Hyper-Rayleigh Scattering Studies of Gold-Core/silver-Shell Nanoparticles: Comparisons of Theory and Experiment. *Chem. Phys. Lett.* **2002**, *352*, 421−428.
(49) Mulvaney, P. Surface Plasmon Spectroscopy of Nanosized Metal Particles. *Langmuir* **1996**, *12*, 788−800.
(50) Gonçalves, M. R. Plasmonic Nanoparticles: Fabrication, Simulation and Experiments. *J. Phys. D: Appl. Phys.* **2014**, *47*, 213001.
(51) Bastús, N. G.; Merkoçi, F.; Piella, J.; Puntes, V. Synthesis of Highly Monodisperse Citrate-Stabilized Silver Nanoparticles of up to 200 Nm: Kinetic Control and Catalytic Properties. *Chem. Mater.* **2014**, *26*, 2836−2846.
(52) Johnson, P. B.; Christy, R. W. Optical Constants of the Noble Metals. *Phys. Rev. B: Solid State* **1972**, *6*, 4370−4379.
(53) Palik, E. D.; Ghosh, G. *Handbook of Optical Constants of Solids*; Palik, E. D., Ed.; Academic Press, 1998; Vol. 3.
(54) Ripken, K. Die Optischen Konstanten von Au, Ag Und Ihren Legierungen Im Energiebereich 2,4 Bis 4,4 eV. *Z. Phys. A: Hadrons Nucl.* **1972**, *250*, 228−234.
(55) Segelstein, D. J. The Complex Refractive Index of Water. Masters Thesis, University of Missouri Kansas City, Missouri, USA, 1981.
(56) Kyung, K.-H.; Fujimoto, K.; Shiratori, S. Control of Structure and Film Thickness Using Spray Layer-by-Layer Method: Application to Double-Layer Anti-Reflection Film. *Jpn. J. Appl. Phys.* **2011**, *50*, 035803.
(57) Haiss, W.; Thanh, N. T. K.; Aveyard, J.; Fernig, D. G. Determination of Size and Concentration of Gold Nanoparticles from UV−Vis Spectra. *Anal. Chem.* **2007**, *79*, 4215−4221.
(58) Fang, Y.; Seong, N.-H.; Dlott, D. D. Measurement of the Distribution of Site Enhancements in Surface-Enhanced Raman Scattering. *Science* **2008**, *321*, 388−392.
(59) Tian, J.-H.; Liu, B.; Li, X.; Yang, Z.-L.; Ren, B.; Wu, S.-T.; Tao, N.; Tian, Z.-Q. Study of Molecular Junctions with a Combined Surface-Enhanced Raman and Mechanically Controllable Break Junction Method. *J. Am. Chem. Soc.* **2006**, *128*, 14748−14749.
(60) *Surface-Enhanced Raman Scattering*; Kneipp, K., Moskovits, M., Kneipp, H., Eds.; Topics in Applied Physics; Springer Berlin Heidelberg, 2006; Vol. *103*.

DOI: 10.1021/acsami.7b13965
ACS Appl. Mater. Interfaces 2017, 9, 41577−41585